University of Birjand

Water Harvesting Research (2026) Vol. 9, No. 1: 155-169

10.22077/jwhr.2026.11928.1212

ORIGINAL ARTICLE

Integrated Urban Fluvial Flood Risk Assessment: A Source–Pathway–Receptor–Consequence (SPRC) Application in Qazvin, Iran

Bahareh Hossein-Panahi[a], Seiyed Mossa Hosseini[b*], Elahe Kakavand[c]

[a]Department of Irrigation and Reclamation Engineering, Faculty of Agricultural Engineering and Technology, College of Agriculture and Natural Resources, University of Tehran, Karaj, Iran.
[b]Physical Geography Department, University of Tehran, P.O. Box: 14155-6465, Tehran, Iran.
[c]Senior Engineering, Regional Water Company of Qazvin, Qazvin, Iran.

[*]Corresponding Author E-mail Address: smhosseini@ut.ac.ir
Received: 23 August 2026, **Revised**: 04 September 2026, **Accepted**: 15 September 2026

Abstract

Flood risk assessment in developing regions is often constrained by the absence of locally derived depth–damage functions, limiting the reliability of loss estimation and risk-informed planning. This study proposes an integrated methodology that combines the Source–Pathway–Receptor–Consequence (SPRC) framework with socio-economic indicators to assess fluvial flood risk in the Shotorak catchment, Qazvin Province, Iran. In the absence of local damage data, European Commission depth–damage curves were applied to hydraulic simulation outputs for 25- and 100-year return period flood events. The modelling results indicate maximum flood depths of 5.85 m and 11.02 m, with inundation extents of 29.79 ha and 45.67 ha, respectively. Residential land in Mohammadieh was affected over 3.4 ha under the 25-year scenario and 5.9 ha under the 100-year scenario, while agricultural land in Sharifieh experienced the greatest losses, increasing from 12.5 ha to 17.4 ha. Residential risk increased by 52% between the two scenarios, underscoring the exposure of expanding urban settlements. The findings reveal pronounced spatial variability in flood impact, driven by the interplay of topography, land use, and socio-economic conditions. Overall, the proposed framework offers a transferable and practical interim tool for flood risk screening and risk-sensitive planning in regions where local depth–damage functions are unavailable.

Keywords: Depth–damage curves, Flood risk assessment, Fluvial flood, Hydraulic modelling, Vulnerability.

1. Introduction

Flooding poses a significant risk to urban areas, particularly in regions with concentrated infrastructure and populations (Nicholls 2015). The growth rate of populations residing in flood-prone regions has exceeded previous scientists' expectations (Khojeh et al. 2022), with the global population in such areas increasing by 34.1% between 2000 and 2015, compared to an 18.6% increase in the global population overall (European Environment Agency 2016). According to the United Nations Office for Disaster Risk Reduction (UNISDR), floods accounted for 47% of all documented natural disasters between 1995 and 2015, affecting 2.3 billion people worldwide. Ongoing fluvial flood stressors, including climate change, land use (especially deforestation), and poor land use planning in urban areas is exacerbating flood risks by altering the probability of flood events. Without considering the impacts of climate change, flood damages are projected to exceed US $50 billion per year by 2050 (Taramelli et al. 2022).

In Iran, rapid urbanization has significantly intensified flood risks, especially in areas with inadequate housing and infrastructure. Recent studies have shown that the increasing urban population is a major factor contributing to this

vulnerability (e.g., Khojeh et al. 2022; Behzadi et al. 2024). The urban population in Iran was 75.94% in 2019 and is projected to reach 85.82% by 2050, much higher than the global urban population rate of 55% in the same period (UN 2016).

Flood risk is a function of the interaction between hazard (the probability and characteristics of flood events), vulnerability (the potential for losses and recovery capacity), and risk levels. A robust risk assessment framework is essential for quantifying these components and facilitating effective flood prevention strategies (Cançado et al. 2008). Risk-based analysis of fluvial floods in urban areas can help resolve conflicts between the value of assets/land uses in floodplains and the costs of protecting those (Auliagisni et al. 2022). The EU Floods Directive defines flood risk as the combination of the probability of a flood event and its potential adverse consequences for human health, the environment, cultural heritage and economic activities.

Over the past two decades, systems-based approaches to flood risk assessments in urban areas have gained prominence (e.g., Ziya and Safaie 2023). One widely used method for assessing flood risk is the Crichton Risk Triangle, which integrates hazard, vulnerability, and exposure (Kron 2005). Flood risk assessment and mapping are critical for designing protection structures and ensuring the safety of people and their socio-economic activities (Taramelli et al. 2022). To better understand the relationship among the flood source, flood protection structures, land area, and stakeholders, a conceptual approach is needed. This framework is widely used in hydraulic engineering, particularly in flood risk assessment, to provide a better understanding of each element of risk analysis because of its simplicity, inherent flexibility, and ability to capture system linkages during flood events (Bakewell and Luff 2008).

Understanding the multidimensional nature of vulnerability and exposure is essential for flood risk evaluation and for implementing effective risk management strategies (Morelli et al. 2021). Flood vulnerability refers to the susceptibility of individuals, communities, infrastructure, or ecosystems to the impacts of flooding, considering both exposure to flood hazards and the capacity to cope with or recover from these impacts. It is commonly assessed through both quantitative and qualitative approaches, including the evaluation of physical, social, economic, and environmental factors that influence vulnerability (Ros et al. 2024). In the literature, two primary approaches are used for assessing flood vulnerability and consequences:

1) Depth-damage functions: These functions, which estimate damage based on flood depth, are widely used in quantitative flood risk analysis. However, they rely on local or global depth–damage curves (as a measure of susceptibility) and estimate maximum possible damage, which can lead to uncertainties in the direct assessment of damage (European Environment Agency 2016). In this approach, the vulnerability map is calculated using specific local/global depth–damage curves, e.g., those developed by the European Commission (Huizinga et al. 2017).

This is accomplished through the use of relative damage functions, which provide the expected degree of damage, usually as a function of inundation depth (Ballesteros et al. 2018). Many countries have developed flood depth-damage curves based on the analysis of past flood events and expert judgment (Taramelli et al. 2022).

2) Indicators-based assessments: These approaches use specific indicators to characterize flood hazards and their consequences, particularly in regions that lack depth-damage curves (e.g., Ballesteros et al. 2018). Indicators allow for the integration of multiple flood risk components into a single assessment, with the highest vulnerability and damage typically assigned to infrastructures such as urban areas and industrial zones, while areas without human occupation are considered less exposed and are given the lowest value (e.g., Ballesteros et al. 2018; Perini et al. 2016, Ali et al. 2024, Bhere and Reddy 2022).

Despite these advancements, a significant gap remains in the literature: the lack of a standardized methodology that integrates the Source-Pathway-Receptor-Consequence (SPRC) framework with socio-economic indicators. This gap has led to inconsistencies in flood risk assessments (Ajtai et al. 2023). While socio-economic factors—such as land

use patterns, urbanization trends, and development dynamics—are widely recognized as critical determinants of future flood risk (Hamers et al. 2024), they remain insufficiently incorporated into existing risk assessment frameworks. This oversight underscores the need for a more comprehensive approach that systematically bridges the SPRC framework with socio-economic dimensions to enhance the accuracy and reliability of flood risk evaluations. This study addresses this gap by developing a standardized methodology that integrates the SPRC framework with socio-economic indicators for flood risk assessment.

Focusing on Qazvin County, Iran, this research is the first to apply depth-damage functions developed by the European Commission within the Iranian context to evaluate flood vulnerability and potential consequences. By combining the SPRC framework with socio-economic indicators, this study provides a more comprehensive and integrated approach to flood risk assessment. The proposed methodology not only enhances the understanding of flood risks but also supports informed decision-making and the development of effective flood mitigation strategies, aligning with Iran's National Plan of Integrated Flood Management.

2. Materials and Methods

The research flowchart followed in this study is shown in Fig. 1. Three phases—hazard, vulnerability, and risk analysis—were performed, as explained in detail in the subsequent sections. The superposition of different components of the SPRC model with the three phases considered in this study is also illustrated in Fig. 1.

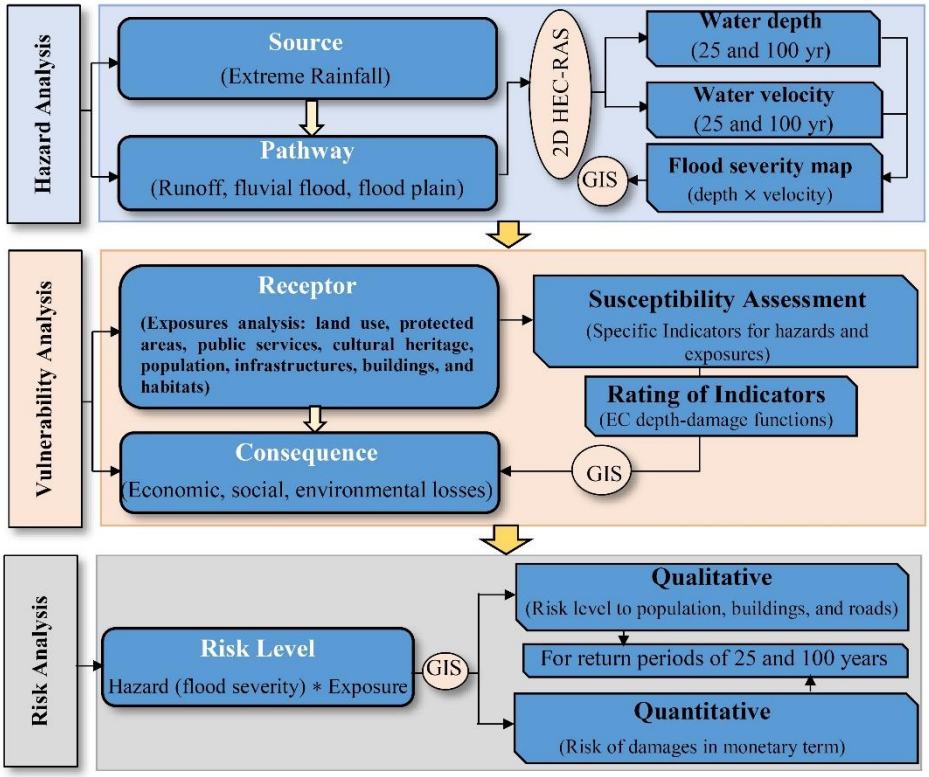

Fig. 1. The Source-Pathway-Receptor-Consequence (SPRC) model for fluvial flood risk assessment.

2.1. Study area

The study area is the Shotorak mountainous catchment located in Qazvin province in northern Iran (Fig. 2). The area of the catchment upstream of Sharifieh town is 125 km^2, the perimeter of the basin is approximately 161 kilometers, and the elevation ranges between 1032 and 2597 m above mean sea level (with an average of 2001 m). The drainage density, Gravelius compactness coefficient, and average slope of the catchment are 6.4, 4.0, and 19.3%, respectively. The average annual precipitation, temperature, and evaporation from surface water bodies in this catchment are 390 mm, and 12 °C, and 1133 mm, respectively. The climate of the study area is semi-arid. Geologically, the middle part of the catchment

contains conglomerate, marl, and sandstone. Gray basalts, andesite, volcanic lava, and tuff are among the dominant geological formations upstream of the catchment. The time of concentration of the study catchment is approximately 2.5 hours (obtained by Kirpich's formula). The average annual streamflow of the studied catchment is 6.8×10^6 m^3 (with the highest runoff occurring in April). Nearly 92.5% of the total streamflow (approximately 6.3×10^6 m^3) is generated by direct runoff from precipitation (Bolourchi 1978; Mosaffaie et al. 2015). The probability distribution of Log-Pearson Type III was the best-fitted distribution for the annual maximum streamflow dataset recorded at the hydrometric station upstream of the study reach over a 30-year observation period. Using this probability distribution, the peak discharge values corresponding to the 25- and 100-year return periods were estimated as 50 and 79 m^3/s, respectively. These peak discharge values were subsequently used as the design flood discharges for the hydraulic simulations.

The probability distribution of Log-Pearson Type III was the best-fitted distribution for the annual maximum streamflow dataset recorded at the hydrometric station upstream of the study reach over a 30-year observation period. Using this probability distribution, the peak discharge values with return periods of 25 and 100 years were estimated to be 50 and 79 m^3/s, respectively.

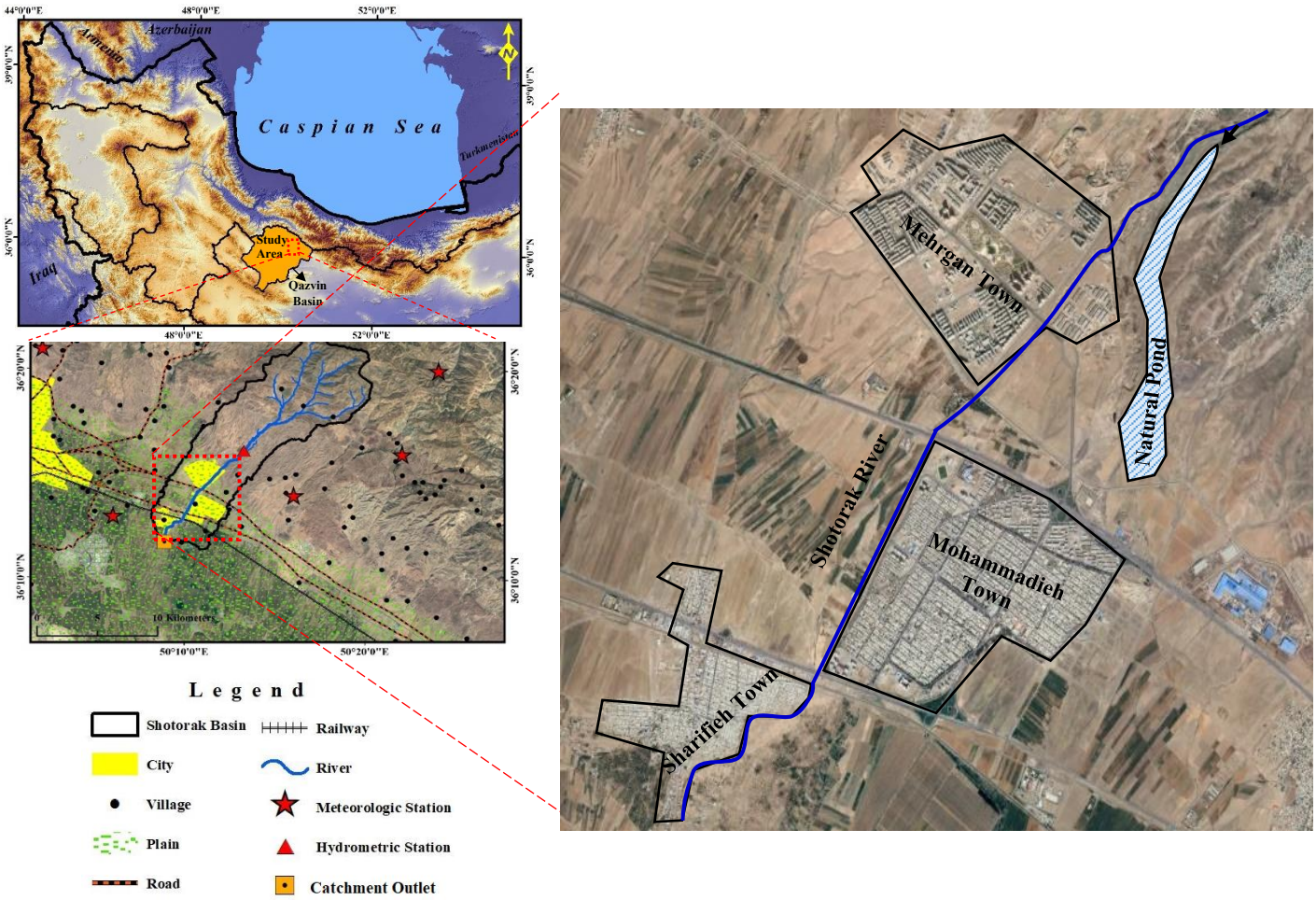

Fig. 2. Location of the Shotorak river catchment and three new-built towns around the river.

In this study, 12 km of the Shotorak River was considered as the study reach, with four bridges located along it. The existence of three newly built towns (Mehrgan, Mohammadieh, and Sharifieh) in the vicinity of this river, along with agricultural lands, highlights the need for flood risk assessment. Floods in this catchment are primarily caused by torrential runoff from the mountainous upstream area to the downstream lowlands.

Despite experiencing several extreme floods, the Shotorak River region has not yet been subjected to a flood risk assessment.

As shown in Fig. 2, there is a natural depression (geological hole) upstream of the study reach (in front of Mehrgan town) which has recently been used as a flood storage pond by Qazvin's regional water authority. An uncontrolled spillway was installed at the entrance of the pond, so that when the river's flood level reaches a certain height, the flood flow is diverted into the pond. In addition to storing part of the flood flow, this pond is also utilized for tourist purposes during non-flood seasons. Despite the implementation of this flood storage pond, the newly built towns around the study river have still experienced destructive floods.

2.2. Field-based validation of hydraulic results

The simulated inundation extent and major flow pathways were qualitatively validated using evidence from previous flood events. Field inspections were conducted together with experts from the Qazvin Regional Water Authority during the project implementation. Residual flood traces, sediment/debris deposits, and other identifiable flood marks from previous events were documented and compared with the simulated inundation boundaries and flow-concentration zones. The comparison indicated consistency between the principal observed flood pathways and the simulated flood-prone areas.

2.3. SPRC conceptual model

The SPRC concept is widely used by researchers to evaluate the flood risk through the linkage between four components (e.g., Khojeh et al. 2022): 1) Sources (e.g., meteorological events) that determine the origin of the hazard; 2) Pathways (e.g., wave propagation, inundation, routes, or overtopping of floods in the river channel); 3) Receptors, which are the elements at risk, including subjects (population) and objects (buildings, roads, land-use), that determine the exposure in the risk model; and 4) 'Negative' consequence (e.g., loss of life, stress, economic loss, environmental degradation, and depreciation of all assets), which determines the vulnerability.

As shown in Fig. 3, this study performs two main consecutive analyses—hazard and vulnerability— to quantify the risk levels associated with different land uses located in the flooded areas, as discussed in the subsequent sections.

2.4. Flood hazard analysis

In this study, the flood hazard map is obtained by combining the depth and velocity of fluvial flash floods. Two flood events were considered: a 25-year return period (Q25) and a 100-year return period (Q100), derived from recorded hydrometric data and fitted with the Log-Pearson Type III distribution. The parameters of these events are summarized in Table 1. Accurate estimation of flood depth and velocity, both in the channel and on the floodplain, is crucial for quantifying the hazard map in terms of flood severity. Two flood events with medium probability (25-year return period) and low probability (100-year return period), following (Dawo 2022), were selected for analysis in accordance with the EU Floods Directive.

The 2D HEC-Geo-RAS model version 6.1 (Gary 2020) is used to simulate the hydraulic characteristics of flood events (e.g., flood extent area, depth, and velocity) in the studied river reach. This phase corresponds to the pathway component in the SPRC approach.

Table 1. Flood event parameters for 25- and 100-year return periods.

Return Period	Peak Discharge (m^3/s)	Rainfall Type	Notes
25 years (Q25)	50	Torrential convective rainfall	Based on hydrometric station records
100 years (Q100)	79	Torrential convective rainfall	Estimated with Log-Pearson III distribution

The DEM used in the 2D HEC-RAS model was derived from high-resolution UAV topographic surveys with an original spatial resolution of 1 m. These data were used to characterize the channel cross-sections and floodplain topography and were aggregated to a 10-m computational grid for the hydraulic simulations. To better represent major flow-controlling features, 5-m breaklines were introduced along the main river channels and roads. The hydraulic model calculated flood depth and velocity using this computational representation, and the resulting hydraulic variables were evaluated at a 5-m spatial resolution. Thus, the 1-m resolution represents

the original topographic data, 10 m represents the base computational grid, and 5 m represents the refined breakline and hydraulic-output resolution. The final risk maps were represented at 0.5 × 0.5 m for cartographic visualization and spatial representation; this finer map resolution does not imply additional hydraulic information beyond that contained in the 5-m hydraulic outputs. It is important to note that HEC-RAS computes the geometric and hydraulic features for each cell and each cell face to capture the sub-grid topography (Khojeh et al. 2022). Known peak discharges corresponding to the 25- and 100-year return periods (50 and 79 m^3/s, respectively) were prescribed as the upstream boundary conditions for the hydraulic simulations, while normal water depth was specified at the downstream boundary. Because the hydraulic analysis was conducted using peak discharge boundary conditions, event hydrographs and flood-volume estimates were not used as inputs to the simulations.

Manning roughness coefficients for channel and floodplain areas, along with on-ground surveying of channel cross-sections and floodplain topography by Unmanned Aerial Vehicle at a resolution of 1 m (comprising 290 cross-sections with an average spacing of 60 m, each cross-section including approximately 500 data points), are among the model inputs. The shallow water equation with a variable time step was used to simulate steady-state supercritical 2D flood propagation. Simulated values of flood depth and velocity for each 5-m pixel were used to calculate the hazard index (HI) in terms of flood severity:

$$HI_j = d_j \times v_j \quad (1)$$

Where HIj represents the flood severity for pixel j, d_j and v_j are the average flood depth (m) and flow velocity (m/s), respectively, for pixel j. The unit of HI_j is square meters per second (m^2/s). Equation 1 was applied to the inundated areas for the 25- and 100-year flood scenarios. Some researchers (e.g., Krvavica et al. 2023) have categorized HI_j values into different severity classes: $HI_j < 0.05$ (minor severity, people expected to survive), $0.05 < HI_j < 0.15$ (low severity, people in danger), $0.15 < HIj < 0.25$ (medium severity, floating objects), $0.25 < HI_j < 0.35$ (high severity, high risk for people outdoors and low risk for buildings), and $HI_j > 0.35$ (extreme severity, structural damage to buildings). The study reach was 12 km long and included four bridges. Hydraulic modeling inputs are summarized in Table 2, which details river geometry, DEM data, and Manning's roughness coefficients.

Table 2. Hydraulic and geometric parameters used in 2D HEC-GeoRAS modeling.

Parameter	Value/Range	Source/Notes
Selected river reach length	12 km	Shotorak River, upstream to downstream section
DEM resolution	1 m (UAV survey), aggregated to 10 m grid	UAV-based topographic mapping
Number of cross-sections	290	Average spacing: 60 m
Points per cross-section	~500	UAV and field survey
Manning's n (channel)	0.050–0.055	Calibrated using field obs.
Manning's n (floodplain)	0.045–0.050	Calibrated using land use
Time of concentration	2.5 hours	Kirpich's formula

2.5. Flood vulnerability analysis

Flood vulnerability is a multi-dimensional, dynamic, scale-dependent, and site-specific concept in risk assessment, defined as a function of the character and magnitude of flooding, the extent to which a system is exposed, and the sensitivity and adaptive capacity of that system (Nicholls et al. 2015). Flood vulnerability is commonly represented in the form of economic damage curves, which imply the relationship between the levels of damage to a specific type of element at risk and a given level of hazard intensity (Englhardt et al. 2019).

Vulnerability information for public facilities such as emergency services, educational facilities, transportation, cemeteries, etc. was obtained from field investigations and Google Maps (using Google Earth Engine) and refined through manual digitization. The vulnerability assessment, which includes the two last components of SPRC model (receptors and consequence), is defined as the potential for a particular class of buildings or infrastructure facilities to be affected or damaged under a given flood intensity.

Each exposure indicator was represented using an ordinal rating scale from 1 to 5, where 1 denotes very low exposure and 5 denotes

very high exposure. The ratings were assigned according to the relative significance of each receptor category within the flood-risk system. Thus, residential, commercial, industrial, transport, public infrastructure, agricultural, protected-area, and cultural-heritage receptors were represented using a common 1–5 scale. Because all indicators were already expressed on the same ordinal scale, no additional normalization was applied before aggregation. These scores represent relative exposure levels, rather than physical or monetary quantities.

The consequences of flood hazard can be quantified by a set of socio-economic indicators for the main land-use exposures including residential building (E_{RB}), commercial buildings (E_{CB}), industry (E_{Ind}), transport services (E_{TS}), public infrastructure (E_{PI}), agricultural lands (E_{AL}), protected areas (E_{PA}), and cultural heritage (E_{CH}). These are aggregated into an Exposure Index (EI) through the geometric mean:

$$\begin{aligned} EI_k = [&(E_{RB})_k \times (E_{CB})_k \times (E_{Ind})_k \\ &\times (E_{TS})_k \times (E_{PI})_k \\ &\times (E_{AL})_k \times (E_{PA})_k \\ &\times (E_{CH})_k]^{\frac{1}{n}} \end{aligned} \quad (2)$$

For a better representation of the results, the floodplain area was divided into k different zones according to the municipality units. In Eq. 2, an absent exposure category is treated as not applicable, rather than as a numerical zero. Therefore, only exposure categories that are actually present in zone k are included in the product, and n represents the number of applicable exposure categories in that zone. This treatment ensures that the absence of one receptor type does not artificially reduce the overall Exposure Index to zero. For each exposed land-use category, maximum potential damage was adjusted by a depth–damage curve specific to that category and the flood severity at that location. The EI values were computed at the land-use scale in the floodplain areas, whereas the HI values, at the pixel size of 5 m, were averaged for each corresponding land-use.

In what follows, the depth-damage functions used for quantifying the exposures categories for which such functions were available are presented.

2.6. Flood depth-damage functions

Damage functions describe the relationship between economic damage and flood severity (here, the combination of water depth and velocity) and can be derived by accounting for the effects of a flood in terms of asset depreciation (Notaro et al. 2014). Unfortunately, Iran still does not have an officially nationwide depth-damage curve for floods. To overcome this limitation, the commonly used depth–damage curves developed by the European Commission are utilized for each land-use category (Huizinga et al. 2017). Recently, the European Commission developed a global database of fluvial flood depth-economic damage curves for 214 countries worldwide, covering six classes of assets and land use, including residential buildings, commerce, industry, transport, infrastructure, and agriculture (Huizinga et al. 2017).

Flood depth-damage functions from the European Commission, obtained from 14 countries in Asia, were averaged and normalized within the range of 0 to 1 for the damage factor and used in this study (Fig. 3). These curves, shown in Fig. 3, present the percentage of economic exposure values that would suffer damage for different flood depths per land use class. In addition, the exposure of protected areas and cultural heritage in the risk assessment process was accounted for by equating their damage function to that of commercial buildings, which sustain the maximum damage from flood (Fig. 3).

In mathematical terms, the flood risk value (R_k) for each land-use category was obtained by combining Equations 1 and 2 (Ballesteros et al. 2018):

$$R_k = \sum_{k=1}^{N} \sqrt{\mathrm{HI}_k \times \mathrm{EI}_k} \times A_k \quad (3)$$

Where, A_k is the inundated area by the analyzed flood event in zone k, N is the number of zones, HI_k and EI_k are the hazard and exposure index values for zone k as expressed by Equations 1 and 2 . Finally, Eq. 4 (Ballesteros et al. 2018) calculates the value of total risk (R_T) in the inundated area for each flood event:

$$R_T = \frac{\sum_{k=1}^{N}\left(\sqrt{\mathrm{HI}_k \times \mathrm{EI}_k} \times A_k\right)}{\sum_{k=1}^{N} A_k} \quad (4)$$

Both R_k and R_T are dimensionless relative risk indices derived from the

normalized/ordinal hazard and exposure components and should not be interpreted as monetary damage or absolute economic loss estimates. Higher values indicate relatively greater flood-risk levels among the assessed areas and scenarios.

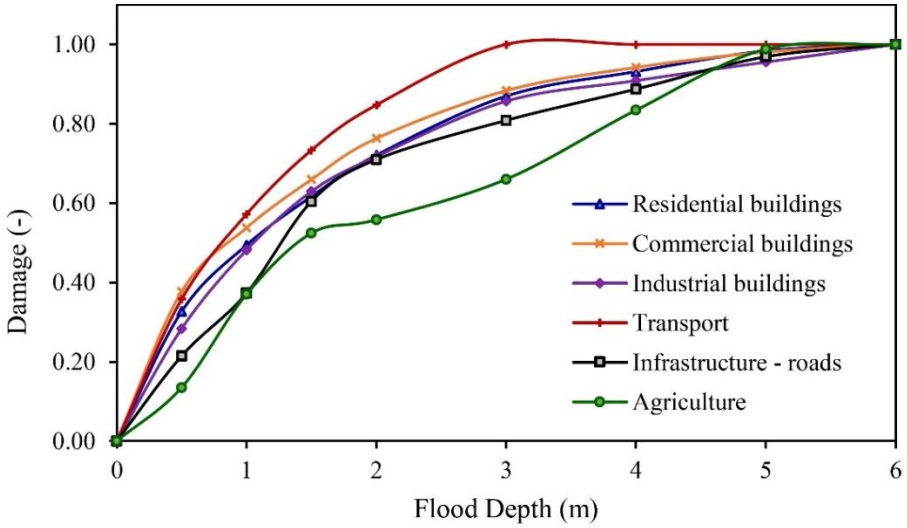

Fig. 3. Average flood depth-damage curves for six impact classes developed by European Commission JRC (April 2017) for the 14 countries of Asia continent.

3. Results and Discussion

Accurate execution of hydraulic models relies heavily on detailed spatial inputs, particularly floodplain and channel cross-sections and Manning's roughness coefficients. In this study, Manning's n values were calibrated based on a combination of land use maps, field observations at flow-disrupting features such as bridges and meanders, and standard reference tables (Phillips and Tadayon 2006). The selected roughness coefficients (0.05–0.055 for channels and 0.045–0.050 for floodplains) played a crucial role in achieving realistic flood simulation outputs, consistent with findings from Aronica et al. (2012) and Lamichhane and Sharma (2018), who emphasized the sensitivity of flood modeling to this parameter.

Figure 4(a–d) presents the spatial distribution of flood depth and velocity for 25-year (50 m^3/s) and 100-year (79 m^3/s) return periods simulated using HEC-Geo-RAS. The maximum simulated flood depth reached 5.85 m under Q25 and 11.02 m under Q100. Importantly, these values represent localized maximum depths, concentrated near the natural topographic depression used as a flood-storage pond upstream of the study reach. The large local depth is therefore associated with topographic storage and flow concentration within this depression and should not be interpreted as a representative inundation depth throughout Mohammadieh town. Outside this localized storage area, simulated depths were substantially lower. Peak flow velocities increased from 5.10 m/s under Q_{25} (Fig. 4c) to 7.0 m/s under Q_{100} (Fig. 4d), indicating greater potential for structural damage and erosion downstream.

The land use map of the study region was prepared using satellite imagery and classified through supervised classification techniques in a GIS environment, supported by field verification and existing land cover datasets to ensure accuracy. Figure 5, classified the study area into residential areas, agricultural lands, and bare lands. Rangeland and roads were not included in the inundated-area totals, while roads and other infrastructure were considered separately in the qualitative risk assessment. Table 3, summarizes inundated areas by land use for each flood scenario. Residential areas in Mohammadieh town were the most vulnerable, with 3.4 ha and 5.9 ha inundated under Q_{25} and Q_{100}, respectively. Agricultural lands in Sharifieh experienced 12.5 ha (Q_{25}) and 17.4 ha (Q_{100}) of flooding, emphasizing the susceptibility of these productive lands to hydrological extremes. To further clarify the flood risk distribution, Table 4 summarizes the elements at risk, inundated areas, and the applied valuation methods.

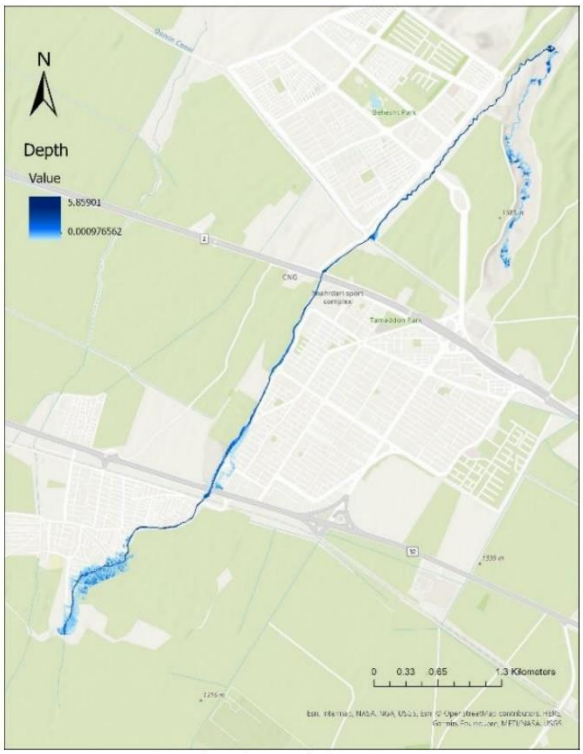

(a) Flood Depth (T= 25-yr)

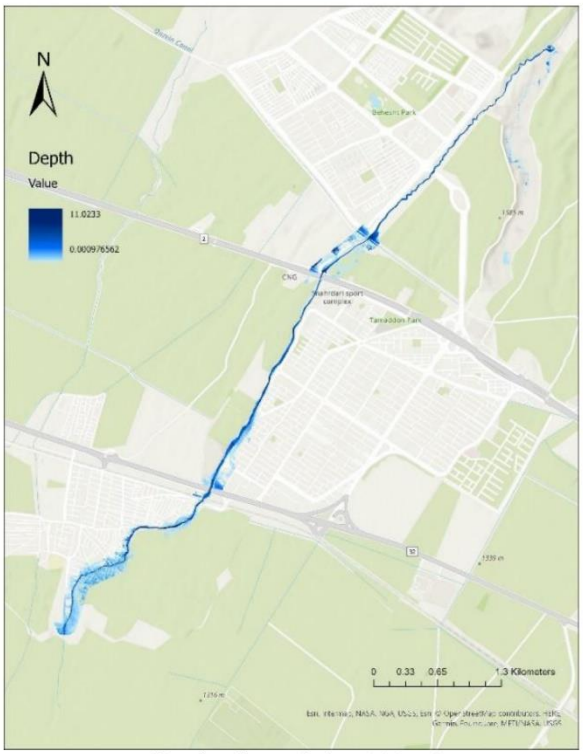

(b) Flood Depth (T= 100-yr)

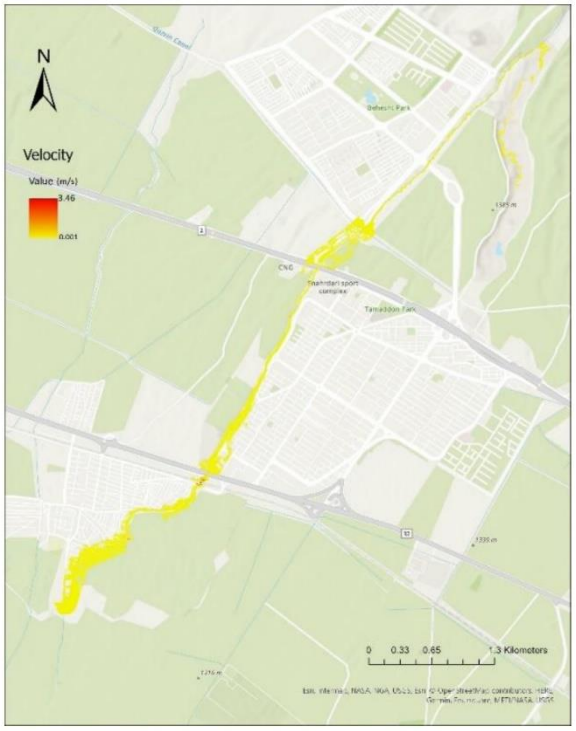

(c) Flood Velocity (T= 25-yr)

(d) Flood Velocity (T= 100-yr)

Fig. 4. Spatial distribution of flood depth and velocity with return period 25-yr and 100-yr simulated by 2D HEC-Geo-RAS model in the studied reach.

Table 3. Inundated areas with different land uses for flood with 25-yr and 100-yr return periods (the values are in hectares).

Town	25-yr return period			100-yr return period		
	Agricultural Lands	Residential Areas	Bare Lands	Agricultural Lands	Residential Areas	Bare Lands
Mehrgan	0.56	0.00	9.57	8.46	0.00	4.23
Mohammadieh	1.59	3.47	0.00	4.18	5.94	0.00
Sharifieh	12.50	2.10	0.00	17.42	5.44	0.00
Sum of Areas	14.65	5.57	9.57	30.06	11.38	4.23

Table 4. Elements at risk, inundated area, and method of valuation.

Land Use / Asset Class	Inundated Area (ha) – Q25	Inundated Area (ha) – Q100	Valuation Method	Notes
Residential (Mohammadieh & Sharifieh)	5.6	11.4	EC depth–damage curves (residential)	Most affected in towns
Agricultural Lands	14.6	30.0	EC depth–damage curves (agriculture)	Highest exposure overall
Bare Lands	9.6	4.2	Not economically valued	Low exposure
Infrastructure (roads, bridges)	Qualitative risk identified	Qualitative risk identified	EC depth–damage curves (transport)	Localized damage near crossings
Cultural Heritage & Protected Areas	Small patches (<1 ha)	Small patches (<1 ha)	Valued using EC commercial curve (max damage)	Assumed highly sensitive

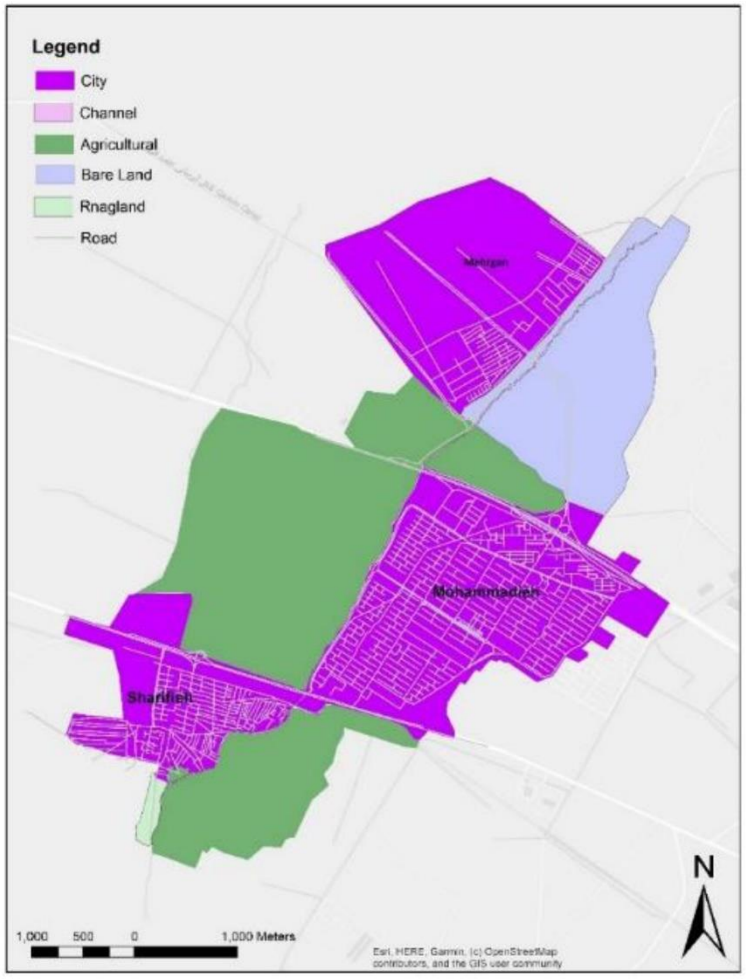

Fig. 5. Land use map of the study area.

The integration of hazard, vulnerability, and exposure within the SPRC framework highlighted that agricultural areas accounted for 66% of high-risk zones, while residential areas contributed 25%. Risk in residential lands increased by 52% between Q25 and Q100, confirming the higher sensitivity of urban settlements compared to other land uses.

Overall, inundated areas increased notably from Q_{25} to Q_{100}, except in upland bare lands of Mehrgan. For the three towns studied, residential inundation increased from 5.57 ha under Q25 to 11.38 ha (Q_{100}), demonstrating the amplification of flood risks with higher discharge scenarios. Agricultural land represented the largest inundated land-use category, with 14.65 ha under Q25 and 30.06 ha under Q100, followed by residential and bare lands (9.6 and 4.2 ha). Exposure maps, derived using the geometric aggregation of the applicable exposure indicators described in Eq. 2, provide further insight into flood-prone zones.

Flood severity, calculated as the product of depth and velocity (Eq. 1), is visualized in Fig. 6(a–b). Severe flooding was primarily concentrated near the river, particularly in Mohammadieh town and in an upstream natural pond acting as a detention basin. The potential effectiveness of such natural retention systems has been demonstrated in other study areas. For example, Lockwood et al. (2022) reported that offline water-storage ponds can attenuate peak flows when appropriately managed.

Annual expected damage for each land use class was estimated using flood depth and standard depth-damage curves (Fig. 3). These damage maps informed the flood risk assessment, which integrated hazard, vulnerability, and exposure via the SPRC framework. Figures 7(a–b) depict spatial flood risk distributions at 0.5×0.5 m resolution. High-risk zones (totaling 45.67 ha) predominantly covered agricultural (66%), residential (25%), and bare lands (9%). Risk escalations were most pronounced in residential areas, where average risk values increased from 1.35 (Q_{25}) to 2.06 (Q_{100}), a 52% surge (Fig. 8), underscoring the sensitivity of urban areas to infrequent but intense floods.

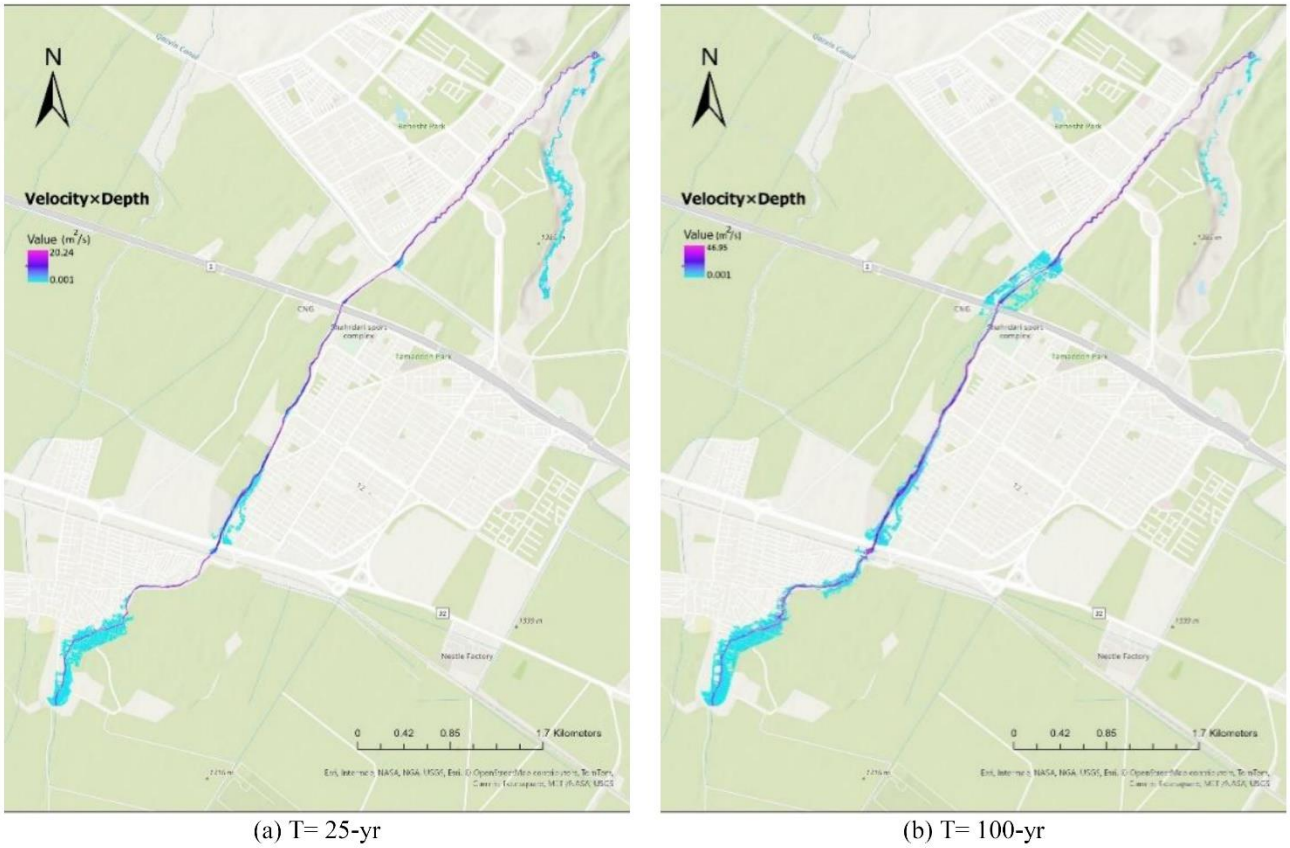

(a) T= 25-yr (b) T= 100-yr

Fig. 6. Flood severity as hazard map with return period 25-yr (a) and 100-yr (b) obtained by product of flood depth and velocity data layers.

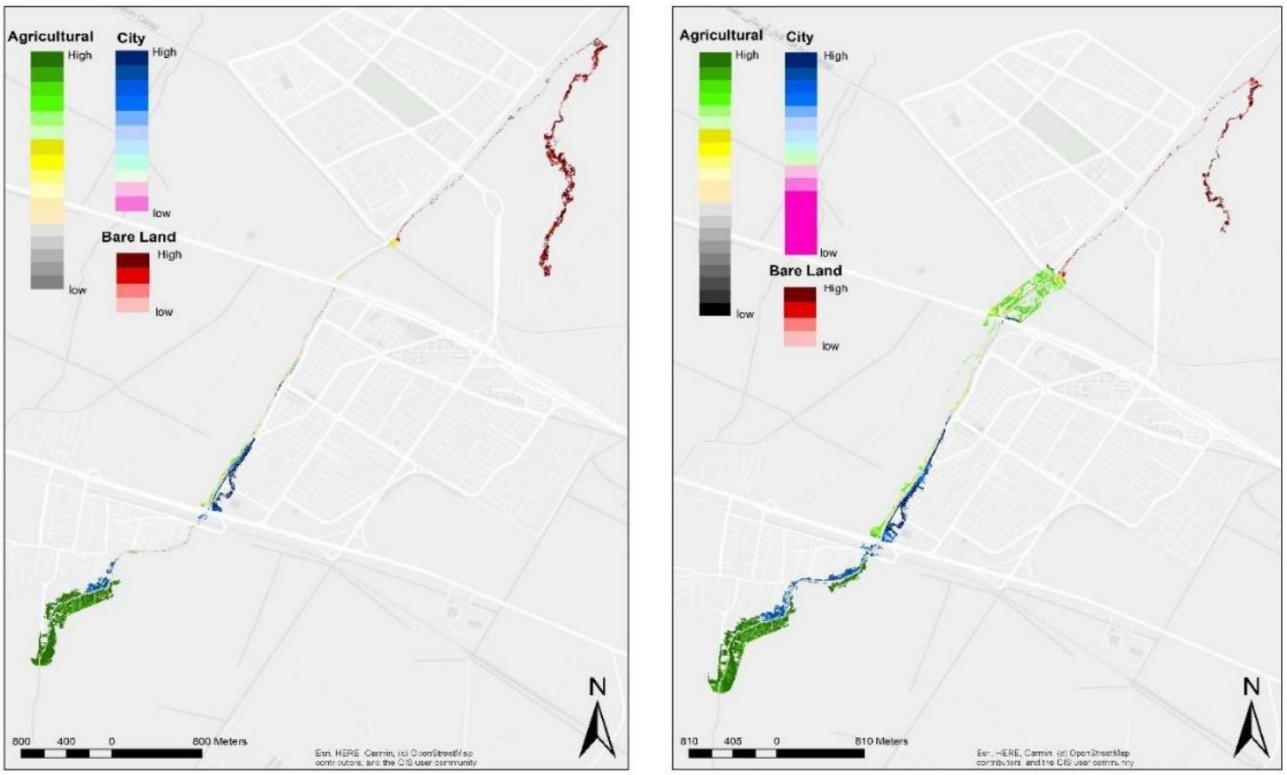

(a) (b)

Fig. 7. Risk map of the study area for the flood with return period of 25-yr (a) and 100-yr (b).

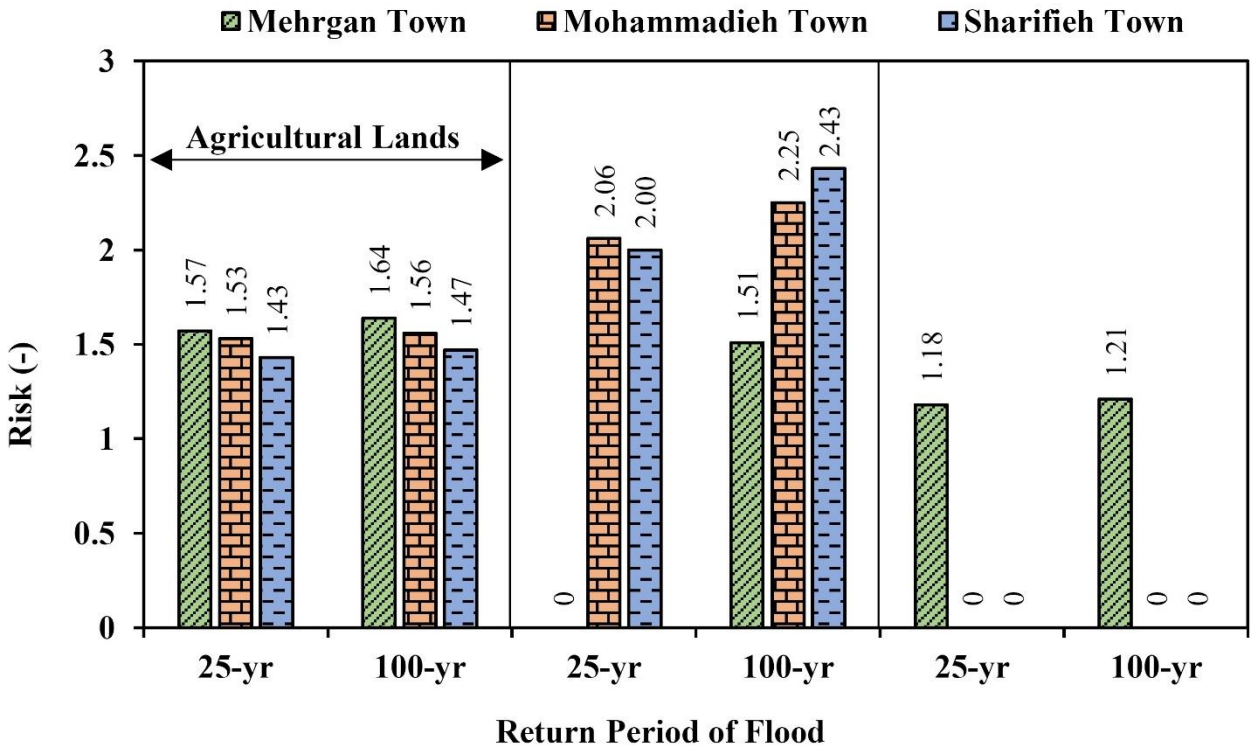

Fig. 8. Summary of the risk of different land use classes (residential, agricultural, and bare lands) in the study area (Mehrgan, Mohammadieh, and Sharifieh towns) for two flood scenarios Q_{25} and Q_{100}.

The discussion underscores that the use of calibrated roughness coefficients, accurate land use classification, and high-resolution hydraulic modeling ensures a robust basis for flood risk analysis. The results are aligned with international literature emphasizing the disproportionate vulnerability of urban and agricultural regions due to impervious surfaces, reduced vegetation, and inadequate drainage systems (Liu et al. 2023).

The SPRC framework facilitated a comprehensive integration of biophysical and

socio-spatial variables. The concentration of high-risk areas along the Shotorak River, especially in Sharifieh town, aligns with prior damage reports and emphasizes the need for enhanced resilience planning. Incorporating socio-economic data improved vulnerability assessment, in line with Bonasia et al. (2024), and highlighted community-specific disparities in exposure and capacity to recover.

Despite the methodological strengths, the study is limited by the use of averaged depth-damage functions from 14 Asian countries, which may not fully reflect local socio-economic conditions. The absence of Iran-specific flood damage functions is a notable gap. Moreover, although the analysis integrates vulnerability, hazard, and exposure, it omits the "response" component, which includes preparedness and adaptive capacity—factors increasingly recognized as critical in integrated risk frameworks (Morgado et al. 2023).

Future work should focus on quantifying soft measures like early warning systems, evacuation planning, and community preparedness. These elements could significantly alter the flood damage curve, particularly for residential zones. Given the increasing urban encroachment into floodplains and the amplified flood risk from climate change, the findings of this study are especially relevant to national policy. Risk maps can guide not only infrastructure investments and emergency planning but also support flood insurance market development and relocation strategies in high-risk zones near megacities.

4. Conclusion

This study presents a comprehensive yet adaptable approach to flood risk assessment in data-scarce mountainous regions by integrating hazard, exposure, and vulnerability components within the Source-Pathway-Receptor-Consequence (SPRC) framework. By employing European Commission depth-damage functions, it offers a practical interim solution in the absence of local damage data, making it applicable in regions like Iran.

The analysis revealed that residential and agricultural areas are particularly at risk, with the 100-year flood scenario causing significantly greater impacts than the 25-year event. The framework effectively identifies high-risk zones and potential flood pathways, supporting prioritization of mitigation and protection strategies.

A major limitation of the study is the lack of region-specific flood depth-damage curves in Iran, which introduces uncertainty into damage estimates. While the European functions provide a useful approximation, they may not accurately reflect local socioeconomic and infrastructure conditions. Future research should focus on developing and validating localized damage functions to improve risk accuracy and relevance.

To enhance the robustness of flood risk assessments, future studies should also address: (1) the influence of climate change and variability on flood dynamics, (2) both tangible and intangible damages (e.g., anxiety damage, social disruption), and (3) the inherent uncertainties in flood modeling and decision-making. These additions will support more comprehensive and resilient flood management policies, particularly in politically sensitive contexts where defining acceptable risk levels remains a critical challenge.

Future studies should further investigate the sensitivity of flood-risk estimates to alternative weighting schemes for exposure indicators. Although the present study follows an SPRC-based aggregation approach using equal weights within the geometric-mean formulation, different receptor categories may have different levels of socioeconomic importance. Therefore, expert-based weighting approaches, such as the Analytic Hierarchy Process (AHP), could be evaluated and compared with the equal-weight approach to examine their effects on the spatial distribution and magnitude of the estimated flood risk.

5. Acknowledgment

The authors appreciate the Qazvin Water Regional Authority for providing the required data for analyses. This work was supported by the Qazvin Water Regional Authority under research project No. 1401/2204/101 (State Code 102380).

6. Conflict of Interest

The authors have no conflict of interest to declare.

7. References

Ajtai, I., Ştefănie, H., Maloș, C., Botezan, C., Radovici, A., Bizău-Cârstea, M., & Baciu, C. (2023). Mapping social vulnerability to floods. A comprehensive framework using a vulnerability index approach and PCA analysis. *Ecological Indicators*, *154*, 110838. https://doi.org/10.1016/j.ecolind.2023.110838

Ali, A., Ullah, W., Khan, U. A., Ullah, S., Ali, A., Jan, M. A., ... & Jan, Q. (2024). Assessment of multi-components and sectoral vulnerability to urban floods in Peshawar–Pakistan. *Natural Hazards Research*, *4*(3), 507-519. https://doi.org/10.1016/j.nhres.2023.12.012

Aronica, G. T., Biondi, G., Brigandì, G., Cascone, E., Lanza, S., & Randazzo, G. (2012). Assessment and mapping of debris-flow risk in a small catchment in eastern Sicily through integrated numerical simulations and GIS. *Physics and Chemistry of the Earth, Parts A/B/C*, *49*, 52-63. https://doi.org/10.1016/j.pce.2012.04.002

Auliagisni, W., Wilkinson, S., & Elkharboutly, M. (2022). Learning from floods—how a community develops future resilience. *Water*, *14*(20), 3238. https://doi.org/10.1016/j.pce.2012.04.002

Bakewell, I., & Luff I. (2008). North London strategic flood risk assessment – Final Report, DEFRA, UK. https://www.walthamforest.gov.uk/sites/default/files/2021-12/ke79-north-london-strategic-flood-risk-assessment.pdf

Ballesteros, C., Jiménez, J. A., & Viavattene, C. (2018). A multi-component flood risk assessment in the Maresme coast (NW Mediterranean). *Natural Hazards*, *90*(1), 265-292. https://doi.org/10.1007/s11069-017-3042-9

Behzadi, F., Javadi, S., Hafezi, S., Vasheghani Farahani, E., & Golmohammadi, G. (2024). Flood risk projection in Iran using CMIP6 models and frequency analysis of precipitation. *Stochastic Environmental Research and Risk Assessment*, *38*(12), 4843-4861. https://doi.org/10.1007/s00477-024-02835-8

Bhere, S., & Reddy, M. J. (2022). Multivariate Flood Risk Assessment of the Unplanned Semi-Urban Region by Incorporating Flood Hazard, Vulnerability, and Exposure. https://doi.org/10.21203/rs.3.rs-1286315/v1

Bolourchi, M. H. (1978). A geological study of the Avaj region (Report No. 6). Geological Survey of Iran. (in Persian)

Bonasia, R., Ceragene, M., Cea, L., & Cuevas Cancino, M. D. L. O. (2024). Crafting Flood Risk Maps and Intensifying Social Vulnerability Studies for Heightened Awareness and Damage Mitigation: Villahermosa, Mexico case. *European Geosciences Union General Assembly 2024 (EGU24)*, 3891. https://doi.org/10.5194/egusphere-egu24-3891

Cançado, V., Brasil, L., Nascimento, N., & Guerra, A. (2008, August). Flood risk assessment in an urban area: Measuring hazard and vulnerability. In *11th International conference on urban drainage, Edinburgh, Scotland, UK* (pp. 1-10). https://www.researchgate.net/profile/Nilo-Nascimento/publication/228507992_Flood_risk_assessment_in_an_urban_area_Measuring_hazard_and_vulnerability/links/0f31753506b5bb838f000000/Flood-risk-assessment-in-an-urban-area-Measuring-hazard-and-vulnerability.pdf

Dawo, L. (2022). *Flood risk assessment in climate change scenarios in the Algarve region* (Master's thesis, Universidade de Lisboa (Portugal)). https://www.proquest.com/openview/d5fdcc6229d4a9ecf1e79a3d4b24ba22/1?pq-origsite=gscholar&cbl=2026366&diss=y

Englhardt, J., De Moel, H., Huyck, C. K., De Ruiter, M. C., Aerts, J. C., & Ward, P. J. (2019). Enhancement of large-scale flood risk assessments using building-material-based vulnerability curves for an object-based approach in urban and rural areas. *Natural Hazards and Earth System Sciences*, *19*(8), 1703-1722. https://doi.org/10.5194/nhess-19-1703-2019

Gary B. (2020) Hydraulic Reference Manual, version 5.0. In HEC-RAS River Analysis System; USACE Hydrologic Engineering Center: Davis, CA, USA, 2016; Available online: https://www.hec.usace.army.mil/software/hec-ras/documentation.aspx

Hamers, E. M., Maier, H. R., Zecchin, A. C., & van Delden, H. (2024). Framework for considering the interactions between climate change, socio-economic development and land use planning in the assessment of future flood risk. *Environmental Modelling & Software*, *171*, 105886. https://doi.org/10.1016/j.envsoft.2023.105886

Huizinga, J., DE, M., & Szewczyk, W. (2017). Global flood depth-damage functions: Methodology and the database with guidelines. EUR 28552 EN. https://doi.org/10.2760/16510

Khojeh, S., Ataie-Ashtiani, B., & Hosseini, S. M. (2022). Effect of DEM resolution in flood modeling: a case study of Gorganrood River, Northeastern Iran. *Natural Hazards*, *112*(3), 2673-2693. https://doi.org/10.1007/s11069-022-05283-1

Kron, W. (2005). Flood risk= hazard• values• vulnerability, water international. *Water Int*, *30*, 58-68. https://doi.org/10.1080/02508060508691837

Krvavica, N., Šiljeg, A., Horvat, B., & Panđa, L. (2023). Pluvial flash flood hazard and risk mapping in Croatia: Case study in the Gospić catchment. *Sustainability*, *15*(2), 1197. https://doi.org/10.3390/su15021197

Lamichhane, N., & Sharma, S. (2018). Effect of input data in hydraulic modeling for flood warning systems. *Hydrological sciences journal*, *63*(6), 938-956. https://doi.org/10.1080/02626667.2018.1464166

Liu, B., Yang, J., Sha, J., Luo, Y., Zhao, X., & Liu, R. (2023). Analysis of runoff according to land-use change in the upper Hutuo River basin. *Water*, *15*(6), 1138. https://doi.org/10.3390/w15061138

Lockwood, T., Freer, J., Michaelides, K., Brazier, R. E., & Coxon, G. (2022). Assessing the efficacy of offline water storage ponds for natural flood management. *Hydrological Processes*, *36*(6), e14618. https://doi.org/10.1002/hyp.14618

Morelli, A., Taramelli, A., Bozzeda, F., Valentini, E., Colangelo, M. A., & Cueto, Y. R. (2021). The disaster resilience assessment of coastal areas: A method for improving the stakeholders' participation. *Ocean & Coastal Management*, *214*, 105867. https://doi.org/10.1016/j.ocecoaman.2021.105867

Morgado, Y., Areu-Rangel, O. S., Silva, R., Miyashita, T., Mori, N., & Tomiczek, T. (2023). Using the SPRC methodology to assess tsunami risk in Zihuatanejo, Mexico. *Coastal Engineering Journal*, *65*(2), 256-276. https://doi.org/10.1080/21664250.2023.2172992

Mosaffaie, J., Akhzari, D., Rashvand, S., & Ataei, J. (2015). Regional flood frequency analysis using multiple regression method (Case study: hydrometric stations of Qazvin province). *Journal of Range and Watershed Managment*, *68*(4), 821-833. https://doi.org/10.22059/jrwm.2015.56964

Nicholls, R., Zanuttigh, B., Vanderlinden, J. P., Weisse, R., Silva, R., Hanson, S., ... & Koundouri, P. (2015). Developing a holistic approach to assessing and managing coastal flood risk. In *Coastal risk management in a changing climate* (pp. 9-53). Butterworth-Heinemann. https://doi.org/10.1016/B978-0-12-397310-8.00002-6

Notaro, V., De Marchis, M., Fontanazza, C. M., La Loggia, G., Puleo, V., & Freni, G. (2014). The effect of damage functions on urban flood damage appraisal. *Procedia Engineering*, *70*, 1251-1260. https://doi.org/10.1016/j.proeng.2014.02.138

Perini, L., Calabrese, L., Salerno, G., Ciavola, P., & Armaroli, C. (2016). Evaluation of coastal vulnerability to flooding: comparison of two different methodologies adopted by the Emilia-Romagna region (Italy). *Natural Hazards and Earth System Sciences*, *16*(1), 181-194. https://doi.org/10.5194/nhess-16-181-2016

Phillips, J. V., & Tadayon, S. (2006). *Selection of Manning's roughness coefficient for natural and constructed vegetated and non-vegetated channels, and vegetation maintenance plan guidelines for vegetated channels in central Arizona*. US Geological Survey. https://doi.org/10.3133/sir20065108

Ros, F. C., Tajuddin, N. F. A., Tarmizi, Z. I. A., Rambat, S., Along, N. Z., & Harun, A. N. (2024). Flood vulnerability index based on indicator approach in assessing flood risk in Selangor, Malaysia. *International Journal of Integrated Engineering*, *16*(4), 16-22. https://doi.org/10.30880/ijie.2024.16.04.003

Secretary-General, U. N. (2016). Report of the open-ended intergovernmental expert working group on indicators and terminology relating to disaster risk reduction. *Proceedings of the Seventy-First Session Agenda Item*, *19*. https://www.undrr.org/publication/report-open-ended-intergovernmental-expert-working-group-indicators-and-terminology

Taramelli, A., Righini, M., Valentini, E., Alfieri, L., Gatti, I., & Gabellani, S. (2022). Building-scale flood loss estimation through enhanced vulnerability pattern characterization: Application to an urban flood in Milano, Italy. *EGUsphere*, *2022*, 1-35. https://doi.org/10.5194/egusphere-2022-225

Ziya, O., & Safaie, A. (2023). Probabilistic modeling framework for flood risk assessment: A case study of Poldokhtar city. *Journal of Hydrology: Regional Studies*, *47*, 101393. https://doi.org/10.1016/j.ejrh.2023.101393

Authors retain the copyright and full publishing rights.
Published by University of Birjand. This article is an open access article licensed under the Creative Commons Attribution 4.0 International (CC BY 4.0)